DOI: 10.1002/ejic.200800776

Metastable $Sr_{0.5}TaO_3$ Perovskite Oxides Prepared by Nanosheet Processing

Keigo Inaba,*[a] Shinya Suzuki,[a] Yuji Noguchi,[a] Masaru Miyayama,[a] Kenji Toda,[b] and Mineo Sato[c]

Keywords: Nanotechnology / Nanostructures / Tantalum / UV/Vis spectroscopy / Surface chemistry

Metastable $Sr_{0.5}TaO_3$ with a perovskite structure was prepared by using layer-structured $H_2Sr_{1.5}Ta_3O_{10}$ by two different processes: direct dehydration and nanosheet processing, and the photocatalytic activities of the obtained structures were investigated for the evolution of H_2 and O_2 from distilled water under UV light irradiation. The average gas evolution rates were 66 μmol h^{-1} (H_2) and 16 μmol h^{-1} (O_2) for $Sr_{0.5}TaO_3$ prepared by direct dehydration, whereas those obtained by nanosheet processing were 126 μmol h^{-1} (H_2) and 33 μmol h^{-1} (O_2). It was shown that nanosheet processing is effective for obtaining metastable $Sr_{0.5}TaO_3$ with high photocatalytic activities.

Introduction

Nanosheets with a two-dimensional single crystal with a thickness of several nm have attracted a great deal of attention as a component material for bottom-up processing from scientific and technological points of view.[1–8] The nanosheets are usually obtained from host layer-structured materials composed of monovalent cations such as Li^+, Na^+, and K^+ and transition-metal-oxide layers. In the layered structure of the host materials, the interlayer spacing between the transition-metal-oxide layers provides an important field through intercalation reactions. The exchange reactions from the monovalent cations to H^+ and/or H_3O^+ followed by the intercalation of organic cations such as tetrabutylammonium ions expand the interlayer spacing of the host materials.[9] These multistep intercalation reactions delaminate the host layered materials, which leads to nanosheets comprising the transition-metal-oxide layers.[10–15] Nanosheets are obtained as colloidal suspensions due to repulsive interactions between them with negative charges. When a colloidal suspension is subjected to titration with acid or cations, the nanosheets are restacked and nonconventional layered compounds with a different stacking structure from the host materials can be established.[16,17]

Bottom-up processing using the nanosheet as a component material, that is, nanosheet processing, can provide a possible root for synthesizing three-dimensional materials with novel disordered structures. The reaction between acid and nanosheets in a colloidal suspension yields restacked layered materials with H^+ and/or H_3O^+ in the interlayer spacing. The dehydration of the protonated compounds triggered by heat treatment at moderate temperatures results in a three-dimensional network not only with a large amount of structural imperfections but also in a metastable state. In this paper, metastable $Sr_{0.5}TaO_3$ perovskite oxide obtained by nanosheet processing is reported and the activity of photocatalytic water splitting is investigated.

Photocatalytic water splitting has attracted much attention, because this technology can provide a clean and renewable source for hydrogen fuel. Perovskite-structured oxides with TiO_6,[18–21] NbO_6,[16,22–24] and TaO_6[22,25–37] octahedra have been reported to show high activity in photocatalytic reactions. Particularly, TaO_6 systems such as $LiTaO_3$, $NaTaO_3$, and $KTaO_3$ can produce stoichiometric amounts of H_2 and O_2 from distilled water. For the perovskite oxides with TaO_6 octahedra, the bandgap is established between the conduction band minimum formed by the Ta 5d bands and the valence band maximum mainly composed of the O 2p band, and the *A*-site cation constitutes nonbonding bands at levels far below the Fermi energy. The Ta base perovskite oxides with similar electronic structures are expected to show superior photocatalytic activity. Therefore, we have chosen metastable $Sr_{0.5}TaO_3$ perovskite oxide for photocatalytic water splitting. Electronic structure calculations for $SrTiO_3$ reveal that the electronic bands originating from Sr are present far below the Fermi energy and that the bandgap is built up between the Ti 3d conduction band and the O 2p valence band.[38–40] Because the electronic bands of Sr are low lying from the Fermi energy, the electronic structure of $Sr_{0.5}TaO_3$ is expected to be similar to those of $LiTaO_3$, $NaTaO_3$, and $KTaO_3$.

[a] Research Center for Advanced Science and Technology, The University of Tokyo,
4-6-1 Komaba, Meguro-ku, Tokyo 153-8904, Japan
Fax: +81-3-5452-5083
E-mail: kinaba@crm.rcast.u-tokyo.ac.jp
[b] Graduate School of Science and Technology, Niigata University,
Ikarashi-2, Niigata 950-2181, Japan
[c] Department of Chemistry and Chemical Engineering, Faculty of Engineering, Niigata University,
Ikarashi-2, Niigata 950-2181, Japan

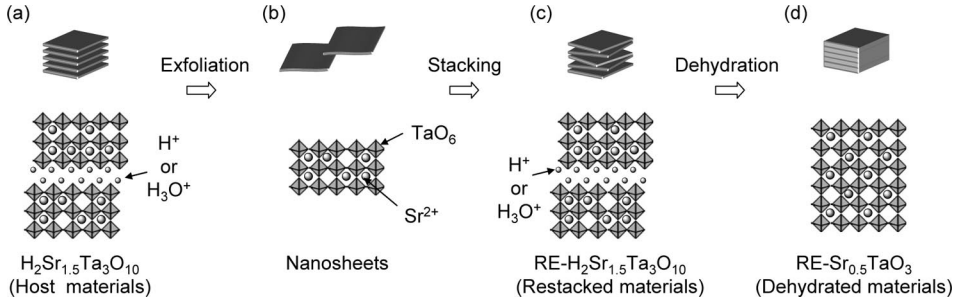

Figure 1. Schematic structural drawing of the transformation from host materials $H_2Sr_{1.5}Ta_3O_{10}$ to dehydrated materials RE-$Sr_{0.5}TaO_3$.

Standard solid-state reactions do not provide $Sr_{0.5}TaO_3$, whereas $Sr_{0.5}TaO_3$ can be obtained from a metastable phase during dehydration of layered perovskite $H_2Sr_{1.5}Ta_3O_{10}$. Here, we synthesized $Sr_{0.5}TaO_3$ through two kinds of different processes: (1) direct dehydration of $H_2Sr_{1.5}Ta_3O_{10}$ and (2) soft chemical stacking of $(Sr_{1.5}Ta_3O_{10})^{2-}$ nanosheets obtained from $H_2Sr_{1.5}Ta_3O_{10}$ (nanosheet processing, see Figure 1). The properties of photocatalytic water splitting for $Sr_{0.5}TaO_3$ prepared by these two different methods are investigated and the higher photocatalytic activity observed for $Sr_{0.5}TaO_3$ obtained from the nanosheets is discussed.

Results and Discussion

Figure 2 shows the XRD patterns of the samples prepared through processes (1) and (2). The peaks observed for $H_2Sr_{1.5}Ta_3O_{10}$ (Figure 2a) at $2\theta \approx 6$, 13, and 19°, which are associated with the layered structure, disappeared after heat treatment (dehydration) at 600 °C for 2 h for $Sr_{0.5}TaO_3$ (Figure 2b). The XRD peaks assigned to the cubic perovskite structure were observed for $Sr_{0.5}TaO_3$ (Figure 2b). These results show that the dehydration of $H_2Sr_{1.5}Ta_3O_{10}$ leads to metastable $Sr_{0.5}TaO_3$ with a perovskite structure. It was found that perovskite $Sr_{0.5}TaO_3$ can be obtained by direct dehydration by using $H_2Sr_{1.5}Ta_3O_{10}$ as the host material.

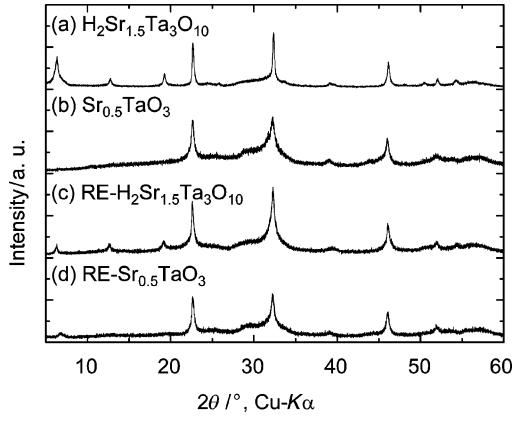

Figure 2. XRD patterns of (a) $H_2Sr_{1.5}Ta_3O_{10}$, (b) $Sr_{0.5}TaO_3$, (c) RE-$H_2Sr_{1.5}Ta_3O_{10}$, and (d) RE-$Sr_{0.5}TaO_3$.

The morphology of $(Sr_{1.5}Ta_3O_{10})^{2-}$ nanosheets used in nanosheet processing was examined by atomic force microscope (AFM). Figure 3 shows an AFM image of the nanosheets: the upper panel is a topographic image and the lower panel is the height profile of the cross section along the white line in the upper panel. The nanosheets had an average height of 4 nm and an average width of 200 nm. From the thickness of the perovskite layers (1.17 nm), the nanosheets appear to be composed of three perovskite layers.

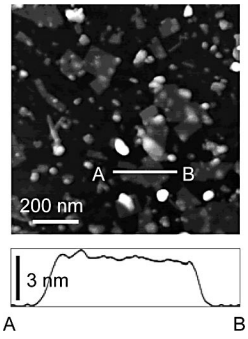

Figure 3. (a) AFM image and (b) height profile of $(Sr_{1.5}Ta_3O_{10})^{2-}$ nanosheets.

Figure 2c exhibits the XRD pattern of RE-$H_2Sr_{1.5}Ta_3O_{10}$ obtained from the reaction between $(Sr_{1.5}Ta_3O_{10})^{2-}$ nanosheets and H^+. The driving force of the reaction is likely the attractive electrostatic interaction between negatively charged nanosheets and positively charged protons. The XRD pattern of RE-$H_2Sr_{1.5}Ta_3O_{10}$ (Figure 2c) is similar to that of $H_2Sr_{1.5}Ta_3O_{10}$ (Figure 2a), showing that RE-$H_2Sr_{1.5}Ta_3O_{10}$ has a layered structure. It was found that RE-$H_2Sr_{1.5}Ta_3O_{10}$ exhibits a broadening of the XRD peaks, which implies the presence of stacking faults induced in the restacking process of $(Sr_{1.5}Ta_3O_{10})^{2-}$ nanosheets. RE-$Sr_{0.5}TaO_3$ (Figure 2d) shows an XRD pattern similar to that of $Sr_{0.5}TaO_3$ (Figure 2b) despite having a peak at $2\theta \approx 6°$, which is attributed to the RE-$H_2Sr_{1.5}Ta_3O_{10}$ residue.

Figure 4 shows the scanning electron microscope (SEM) images of $Sr_{0.5}TaO_3$ and RE-$Sr_{0.5}TaO_3$ particles. $Sr_{0.5}TaO_3$ had plate-like particles with a size of 500 nm, whereas RE-$Sr_{0.5}TaO_3$ possessed smaller particles with a size of 100 nm. The exfoliation performed in nanosheet processing de-

creased the particle size of the products. The surface areas of $Sr_{0.5}TaO_3$ and RE-$Sr_{0.5}TaO_3$ are listed in Table 1. The surface area of RE-$Sr_{0.5}TaO_3$ was 43.4 $m^2 g^{-1}$, which was larger than that of $Sr_{0.5}TaO_3$ (13.5 $m^2 g^{-1}$).

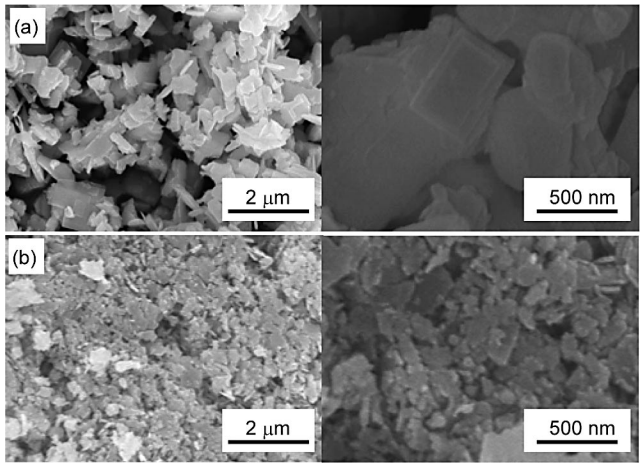

Figure 4. SEM images of (a) $Sr_{0.5}TaO_3$, and (b) RE-$Sr_{0.5}TaO_3$.

Table 1. Photocatalytic activity of $Sr_{0.5}TaO_3$ and RE-$Sr_{0.5}TaO_3$.

Compound	BET surface area [$m^2 g^{-1}$]	Band gap [eV]	Activity [$\mu mol\,h^{-1}$]	
			H_2	O_2
$Sr_{0.5}TaO_3$	13.5	3.7	66	16
RE-$Sr_{0.5}TaO_3$	43.4	3.7	126	44

Figure 5 shows the UV/Vis absorption spectra of $Sr_{0.5}TaO_3$ and RE-$Sr_{0.5}TaO_3$. Both of the samples had an absorbance with a steep edge in the ultraviolet region. The band gap (E_g) can be estimated according to Equation (1).

$$(ahv)^n = A(hv - E_g) \quad (1)$$

where hv is the incident photon energy, a is the absorption coefficient, and A is a constant. The value of n depends on the type of interband transition: $n = 2$ for a direct transition and $n = 1/2$ for an indirect transition. The absorption coefficient is plotted against ($hv - E_g$) in the inset of Figure 5. The slope was estimated to be 2, which shows that RE-$Sr_{0.5}TaO_3$ is classified as an indirect transition material. From the linear extrapolation in Figure 5, the values of E_g were calculated to be 3.7 ($Sr_{0.5}TaO_3$) and 3.7 eV (RE-$Sr_{0.5}TaO_3$). This suggests that the valence band maximum and conduction band minimum are mainly composed of O 2p and Ta 5d bands, respectively. The bands attributed to Sr lie lower in energy than the O 2p valence band. This feature in the electronic structure of $Sr_{0.5}TaO_3$ leads to a constant value of E_g with stacking faults in RE-$Sr_{0.5}TaO_3$, and the same values of E_g were observed for $Sr_{0.5}TaO_3$ and RE-$Sr_{0.5}TaO_3$.

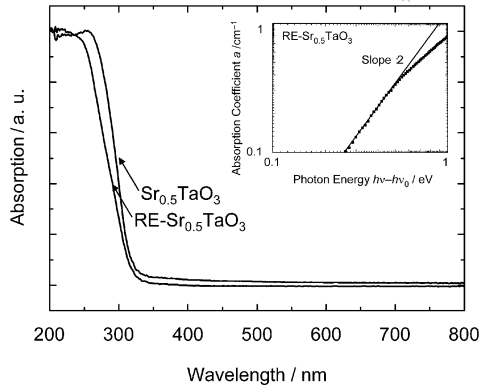

Figure 5. The main panel shows UV/Vis diffuse reflectance spectra of $Sr_{0.5}TaO_3$ and RE-$Sr_{0.5}TaO_3$, with the inset providing a relationship between absorption coefficient and photon energy for RE-$S_{r0.5}TaO_3$.

Figure 6 portrays the photocatalytic gas production from distilled water for 0.5 wt.-% Ni-loaded powders of $Sr_{0.5}TaO_3$ and RE-$Sr_{0.5}TaO_3$. NiO acts as an electron trap and as hydrogen evolution sites. The H_2 and O_2 gases were produced only when light was irradiated onto the samples, whereas gas evolution stopped when the light was turned off (dark reaction). This result indicates that gas evolution is induced by the absorption of light. The average rates of gas evolution were 66 $\mu mol\,h^{-1}$ (H_2) and 16 $\mu mol\,h^{-1}$ (O_2) for $Sr_{0.5}TaO_3$, whereas those of RE-$Sr_{0.5}TaO_3$ were 126 $\mu mol\,h^{-1}$ (H_2) and 33 $\mu mol\,h^{-1}$ (O_2). The nonstoichiometric evolution of H_2 and O_2 probably results from the physisorption and chemisorption of O_2 molecules on the surface of the samples.[36]

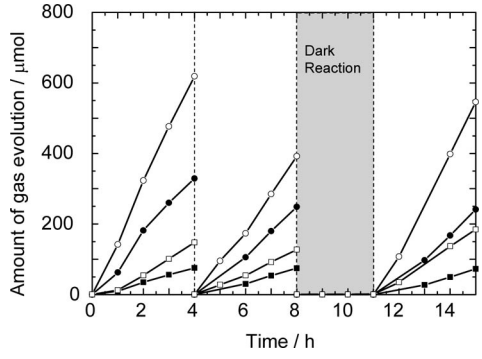

Figure 6. Photocatalytic gas evolution from distilled water dispersed with 0.5 wt.-% Ni-loaded samples: H_2 for $Sr_{0.5}TaO_3$ (●); O_2 for $Sr_{0.5}TaO_3$ (■); H_2 for RE-$Sr_{0.5}TaO_3$ (○); O_2 for RE-$Sr_{0.5}TaO_3$ (□).

One of the possible reasons why $Sr_{0.5}TaO_3$ and RE-$Sr_{0.5}TaO_3$ showed different photocatalytic activities is their different surface areas. RE-$Sr_{0.5}TaO_3$ with a high surface area is likely to have a high density of the site active for the photocatalytic reaction, which resulted in a high photocatalytic activity. Another possible reason is a large number of the stacking faults in RE-$Sr_{0.5}TaO_3$. It is well known that the absorption of photons in photocatalytic materials is accompanied by generation of electron–hole pairs. Photoinduced electron–hole pairs are transferred to the absorbed

water molecules on the surface. Holes in the valence band oxidize absorbed water molecules to produce O_2 gas and hydrogen ions. Electrons in the conduction band reduce hydrogen ions to produce H_2 gas. The local distortions at the stacking faults in RE-$Sr_{0.5}TaO_3$ produce the defect states in the bandgap. The transfer of electrons and holes to the absorbed water molecules might be accelerated through the defect states due to the stacking faults, which is the possible origin of the superior photocatalytic activity of RE-$Sr_{0.5}TaO_3$. In contrast, it is known for TiO_2 that point defects promote recombination of photocarriers generated by optical absorption and then deteriorate the photocatalytic properties.[41] Further investigations on the photocatalytic properties of the samples with different specific surface areas and with different stacking-fault densities are under way. In addition, photoluminescence studies will be conducted to reveal the details of their band structures.

Conclusions

Metastable $Sr_{0.5}TaO_3$ with a perovskite structure was synthesized from layered $H_2Sr_{1.5}Ta_3O_{10}$ as the host material, and the photocatalytic activities of water splitting were investigated for the obtained structures. The photocatalytic activities of $Sr_{0.5}TaO_3$ obtained by nanosheet processing were higher than those of $Sr_{0.5}TaO_3$ prepared by direct dehydration. The superior activities observed for $Sr_{0.5}TaO_3$ obtained by nanosheet processing are suggested to originate from its high surface area and the stacking faults induced during the reassembling of the $(Sr_{1.5}Ta_3O_{10})^{2-}$ nanosheets. Nanosheet processing was found to be effective for synthesizing $Sr_{0.5}TaO_3$ with high photocatalytic activities of water splitting. It is expected that nanosheet processing will provide an efficient means for synthesizing photocatalytic materials of metastable perovskite oxides.

Experimental Section

As a precursor of metastable $Sr_{0.5}TaO_3$, $K_2Sr_{1.5}Ta_3O_{10}$ powder was synthesized by conventional solid-state reaction.[42] The raw materials $SrCO_3$, Ta_2O_5, and K_2CO_3 (40 mol-% excess) were thoroughly mixed and calcined at 850 °C for 6 h and sintered at 1200 °C for 10 h. Ion exchange[43–45] was achieved by treating $K_2Sr_{1.5}Ta_3O_{10}$ with H^+ in 1 M HNO_3 (200 mL). The resulting protonated materials ($H_2Sr_{1.5}Ta_3O_{10}$) were filtered, washed with copious amounts of distilled water, and dried in air. $H_2Sr_{1.5}Ta_3O_{10}$ powder obtained by the above process was designated as the host material (Figure 1a), which was used for synthesizing metastable $Sr_{0.5}TaO_3$ with a three-dimensional perovskite structure (Figure 1d).

$Sr_{0.5}TaO_3$ powder was prepared by two different processes: (1) direct dehydration of the host material[44,46–50] and (2) nanosheet processing (Figure 1). In the direct dehydration process, the host material $H_2Sr_{1.5}Ta_3O_{10}$ was dehydrated by heat treatment at 600 °C for 2 h in air, which led to $Sr_{0.5}TaO_3$ powder. In nanosheet processing, $Sr_{0.5}TaO_3$ was obtained through nanosheets shown in Figure 1b. $H_2Sr_{1.5}Ta_3O_{10}$ (1.6 g) was dispersed in 0.5% tetrabutylammonium hydroxide (TBAOH, 200 mL) aqueous solution with a molar ratio of TBAOH/$H_2Sr_{1.5}Ta_3O_{10}$ = 2:1. The mixture was treated at room temperature for 3 d, which yielded $(Sr_{1.5}Ta_3O_{10})^{2-}$ nanosheets with a thickness of approximately 4 nm (Figure 1b) in the solution. The resulting colloidal suspension of $(Sr_{1.5}Ta_3O_{10})^{2-}$ nanosheets was subjected to centrifugal separation, and the supernatant solution was removed for further use. Excessive amounts of 1-M HCl solution were added into the colloidal suspension to react $(Sr_{1.5}Ta_3O_{10})^{2-}$ nanosheets with H^+. This reaction led to restacking of the $(Sr_{1.5}Ta_3O_{10})^{2-}$ nanosheets into $H_2Sr_{1.5}Ta_3O_{10}$ (Figure 1c). The restacked materials obtained by nanosheet processing are defined as RE-$H_2Sr_{1.5}Ta_3O_{10}$. The precipitates of RE-$H_2Sr_{1.5}Ta_3O_{10}$ were filtered, washed with water, and dried in air. Heat treatment of the precipitates at 600 °C for 2 h transformed RE-$H_2Sr_{1.5}Ta_3O_{10}$ into $Sr_{0.5}TaO_3$ (Figure 1d). The dehydrated materials obtained through nanosheet processing were expressed as RE-$Sr_{0.5}TaO_3$ to differentiate from $Sr_{0.5}TaO_3$ obtained by the direct dehydration of $H_2Sr_{1.5}Ta_3O_{10}$.

X-ray diffraction (XRD) analysis was performed to examine the crystal structure of the samples by using D8 ADVANCE (Bruker AXS) with Cu-K_α radiation. A surface area of the powders was determined by Brunauer–Emmett–Teller (BET) measurements (Shimadzu, TriStar 3000). Nitrogen gas was used as an adsorption–desorption gas. UV/Vis absorption spectra were obtained by the diffuse reflection method by using a spectrometer (Shimadzu, UV-2550), in which $BaSO_4$ was used as a reference. Ni-loaded samples were prepared by the photodeposition method by using $Ni(NO_3)_2$. The properties of photocatalytic decomposition of water were investigated with a gas-closed circulating system. The sample (0.09 g) was dispersed in distilled water (200 mL) by stirring in an inner irradiation cell made of quartz. The light source was a 400-W high-pressure mercury lamp. Before the reaction, the mixture was degassed completely and then Ar was introduced. The amounts of evolved H_2 and O_2 were determined with a gas chromatography (Shimadzu, C-R8A) sampler.

Acknowledgments

We thank Hirotoshi Hatakeyama for determining the photocatalytic activities for the splitting of water. This work was supported by the Global COE Program for Chemistry Innovation.

[1] T. Sasaki, M. Watanabe, H. Hashizume, H. Yamada, H. Nakazawa, *J. Am. Chem. Soc.* **1996**, *118*, 8329–8335.
[2] T. Sasaki, M. Watanabe, H. Hashizume, H. Yamada, H. Nakazawa, *Chem. Commun.* **1996**, 229–230.
[3] T. Sasaki, S. Nakano, S. Yamauchi, M. Watanabe, *Chem. Mater.* **1997**, *9*, 602–608.
[4] T. Sasaki, Y. Ebina, T. Tanaka, M. Harada, M. Watanabe, G. Decher, *Chem. Mater.* **2001**, *13*, 4661–4667.
[5] T. Yamaki, K. Asai, *Langmuir* **2001**, *17*, 2564–2567.
[6] W. Sugimito, O. Terabayashi, Y. Murakami, Y. Takasu, *J. Mater. Chem.* **2002**, *12*, 3814–3818.
[7] L. Wang, T. Sasaki, Y. Ebina, K. Kurashima, M. Watanabe, *Chem. Mater.* **2002**, *14*, 4827–4832.
[8] T. Sasaki, *J. Ceram. Soc. Jpn.* **2007**, *115*, 9–16.
[9] T. Sasaki, M. Watanabe, *J. Am. Chem. Soc.* **1998**, *120*, 4682–4689.
[10] R. E. Schaak, T. E. Mallouk, *Chem. Mater.* **2000**, *12*, 3427–3434.
[11] T. Sasaki, M. Watanabe, *J. Phys. Chem. B* **1997**, *101*, 10159–10161.
[12] Y. Omomo, T. Sasaki, L. Wang, M. Watanabe, *J. Am. Chem. Soc.* **2003**, *125*, 3568–3575.
[13] M. M. J. Treacy, S. B. Rice, A. J. Jacobson, J. T. Lewandowski, *Chem. Mater.* **1990**, *2*, 279–286.

[14] N. Miyamoto, H. Yamamoto, R. Kaito, K. Kuroda, *Chem. Commun.* **2002**, 2378–2379.
[15] A. Takagaki, M. Sugisawa, D. L. Lu, J. N. Kondo, M. Hara, K. Domen, S. Hayashi, *J. Am. Chem. Soc.* **2003**, *125*, 5479–5485.
[16] Y. Ebina, T. Sasaki, M. Harada, M. Watanabe, *Chem. Mater.* **2002**, *14*, 4390–4395.
[17] L. Wang, K. Takada, A. Kajiyama, M. Onoda, Y. Michiue, L. Zang, M. Watanabe, T. Sasaki, *Chem. Mater.* **2003**, *15*, 4508–4514.
[18] T. Takata, Y. Furumi, K. Shinohara, A. Tanaka, M. Hata, J. N. Kondo, K. Domen, *Chem. Mater.* **1997**, *9*, 1063–1064.
[19] S. Ikeda, M. Hara, J. N. Kondo, K. Domen, H. Takahashi, T. Okubo, M. Kakihana, *Chem. Mater.* **1998**, *10*, 72–77.
[20] C. T. K. Thaminimulla, T. Takata, M. Hara, J. N. Kondo, K. Domen, *J. Catal.* **2000**, *196*, 362–365.
[21] T. Tanaka, K. Shinohara, A. Tanaka, M. Hara, J. N. Kondo, K. Domen, *J. Photochem. Photobiol., A* **1997**, *106*, 45–49.
[22] A. Kudo, H. Kato, S. Nakagawa, *J. Phys. Chem. B* **2000**, *104*, 571–575.
[23] Y. Ebina, N. Sakai, T. Sasaki, *J. Phys. Chem. B* **2005**, *109*, 17212–17216.
[24] O. C. Compton, E. C. Carroll, J. Y. Kim, D. S. Larsen, F. E. Osterloh, *J. Phys. Chem. C* **2007**, *111*, 14589–14592.
[25] A. Kudo, H. Kato, *Chem. Lett.* **1997**, *26*, 867–868.
[26] H. Kato, A. Kudo, *Chem. Phys. Lett.* **1998**, *295*, 487–492.
[27] H. Kato, A. Kudo, *Chem. Lett.* **1999**, *28*, 1207–1208.
[28] A. Kudo, H. Kato, *Chem. Phys. Lett.* **2000**, *331*, 373–377.
[29] H. Kato, A. Kudo, *J. Phys. Chem. B* **2001**, *105*, 4285–4292.
[30] Z. G. Zou, J. H. Ye, K. Sayama, H. Arakawa, *Nature* **2001**, *414*, 625–627.
[31] K. Shimizu, Y. Tsuji, M. Kawakami, K. Toda, T. Kodama, M. Sato, Y. Kitayama, *Chem. Lett.* **2002**, *31*, 1158–1159.
[32] H. Kato, K. Asakura, A. Kudo, *J. Am. Chem. Soc.* **2003**, *125*, 3082–3089.
[33] K. Shimizu, Y. Tsuji, T. Hatamachi, K. Toda, T. Kodama, M. Sato, Y. Kitayama, *Phys. Chem. Chem. Phys.* **2004**, *6*, 1064–1069.
[34] K. Shimizu, S. Itoh, T. Hatamachi, T. Kodama, M. Sato, K. Toda, *Chem. Mater.* **2005**, *17*, 5161–5166.
[35] C. C. Hu, H. Teng, *Appl. Catal., A* **2007**, *331*, 44–50.
[36] F. Yao, J. H. Ye, *Chem. Phys. Lett.* **2007**, *435*, 96–99.
[37] Y. C. Lee, H. Teng, C. C. Hu, S. Y. Hu, *Electrochem. Solid-State Lett.* **2008**, *11*, P1–P4.
[38] S. Saha, T. P. Sinha, A. Mookerjee, *J. Phys.: Condens. Matter* **2000**, *12*, 3325–3336.
[39] C. D. Pinheiro, E. Longo, E. R. Leite, F. M. Pontes, R. Magnani, J. A. Varela, P. S. Pizanni, T. M. Boschi, F. Lanciotti, *Appl. Phys. A* **2003**, *77*, 81–85.
[40] T. Tanaka, K. Matsunaga, Y. Ikuhara, T. Yamanoto, *Phys. Rev. B* **2003**, *68*, 205213.
[41] J. Nowotny, T. Bak, M. K. Nowotny, L. R. Sheppard, *J. Phys. Chem. B* **2006**, *110*, 18492–18495.
[42] F. Le Berre, M. P. Crosnier-Lopez, Y. Laligant, J. L. Fourquet, *J. Mater. Chem.* **2002**, *12*, 258–263.
[43] K. Toda, J. Watanabe, M. Sato, *Mater. Res. Bull.* **1996**, *31*, 1427–1435.
[44] N. S. P. Bhuvanesh, M. P. Crosnier-Lopez, H. Duroy, J. L. Fourquet, *J. Mater. Chem.* **2000**, *10*, 1685–1692.
[45] M. P. Crosnier-Lopez, F. Le Berre, J. L. Fourquet, *J. Mater. Chem.* **2001**, *11*, 1146–1151.
[46] V. Thangadurai, G. N. Subbanna, J. Gopalakrishnan, *Chem. Commun.* **1998**, 1299–1300.
[47] R. E. Schaak, T. E. Mallouk, *J. Am. Chem. Soc.* **2000**, *122*, 2798–2803.
[48] R. E. Schaak, T. E. Mallouk, *J. Solid State Chem.* **2000**, *155*, 46–54.
[49] M. P. Crosnier-Lopez, J. L. Fourquet, *Solid State Sci.* **2005**, *7*, 530–538.
[50] F. Le Berre, M. P. Crosnier-Lopez, J. L. Fourquet, *Mater. Res. Bull.* **2006**, *41*, 825–833.

Received: August 4, 2008
Published Online: November 5, 2008

